processes

MDPI

Article

Investigating the Reliability of an Existing Top Angle and Seat Pad Semi-Rigid Connection System Using Advanced Modelling Techniques

Ferid A. Yonis *, Chun-Qing Li and Saman De Saliva *

School of Engineering, University of Royal Melbourne Institute Technology, Melbourne, VIC 3000, Australia; chunqing.li@rmit.edu.au

* Correspondence: fayonis@yahoo.com.au (F.A.Y.); saman.desilva@rmit.edu.au (S.D.S.)

Abstract: The investigation introduces an advanced model procedure for evaluating the structural reliability of semi-rigid frame connections in existing aged buildings. Specifically, the focus is on the top angle and seat pad (TA–SP) semi-rigid connection, which was not initially considered in the current design standards. The approach employs a plastic hinge model to predict the ultimate strength of the connection and its beam-to-column behaviour. In order to increase computational efficiency, the investigation leverages the nonlinear behaviour of the finite element (FE) model to validate critical parameters. The statistical properties of the existing connection were obtained based on past experimental data, highlighting the weakest elements in the system. The first-order and second-order reliability methods and Monte Carlo simulations were employed to estimate the reliability index. Percentile errors were assessed to understand their impact on higher-order interactions. This new technique of identification quantifies the probability of the system failure interactions. Notably, a 45% lesser error aligns with the target reliability index, while a 114.5% larger error indicates a significant deviation from actual failure probability values. Each methodology introduced adheres to the current standard, and the system reliability analysis provides a vigorous conclusions scheme framework for assessing the existing TA–SP semi-rigid connection.

Keywords: semi-rigid connection; M–θ relationship; finite element (FE); locked-chain series system; reliability index; system reliability index; target reliability index

check for updates

Citation: Yonis, F.A.; Li, C.-Q.; Saliva, S.D. Investigating the Reliability of an Existing Top Angle and Seat Pad Semi-Rigid Connection System Using Advanced Modelling Techniques. *Processes* **2024**, *12*, 1221. https://doi.org/10.3390/pr12061221

Academic Editor: Jiaqiang E

Received: 13 March 2024
Revised: 30 May 2024
Accepted: 7 June 2024
Published: 14 June 2024

Copyright: © 2024 by the authors. Licensee MDPI, Basel, Switzerland. This article is an open access article distributed under the terms and conditions of the Creative Commons Attribution (CC BY) license (https://creativecommons.org/licenses/by/4.0/).

1. Introduction

The main purpose of this paper is to assess the reliability of the existing top angle and seat pad (TA–SP) connection, which was widely utilised in high-rise buildings across Australian cities erected from the 1920s to the 1960s. TA–SP connections combine stiffness and flexibility in the frame joints of buildings, presenting unique characteristics. However, despite their prevalence, TA–SP connections lack documented information, and established procedures for analysing their behaviour have not yet been developed.

Typically, TA–SP connections involve multiple elements subjected to tensile and compressive forces, extending beyond their intended purpose of transferring gravity loads only. In traditional analysis methods for steel structures, beam-to-column connections are often idealised as either perfectly rigid or ideally pinned. This is defined as complete displacement and slope continuity between the column and the beam under loading conditions, essentially performing as if it is fixed. On the contrary, the rotation continuity is nonexistent, allowing almost free rotational movement; therefore, they behave as if they are hinged.

Experimental investigations consistently exhibited that perfectly rigid and ideally pinned connections are mostly considered semi-rigid. The assumption of flexibility influences the force distribution among the connected elements, and this behaviour in buildings

is often treated as a semi-rigid frame during analysis. Particularly, modelling the moment–rotation (M–θ) relationship becomes crucial when assessing the semi-rigid connections in the analysis process.

In this context, many numerical models have been developed to assess flexible connections, offering valuable insights into the underlying system. For example, Hardy Cross [1] is accredited first for his contributions to understanding structural behaviours and the flexible rotation of frame connections. Since then, substantial experimental and numerical research has been carried out in the context of developing semi-rigid connections. In the early design development stages, riveted, bolted, and welded connections contributed to how the semi-rigid connections partially transfer moment and share forces between beams and columns, representing their strength, stiffness, and ductility under various loading conditions. This information is now well-established and integral to design methods. Codes such as AISC-LRFD [2] and Eurocode 3 [3] provide deep insights into design models that consider moment–rotation relationships. The application of design parameters such as the initial stiffness (*Rki*), ultimate moment capacity (*Mu*), and shape parameter (*n*) is essential in understanding the semi-rigid connection behaviours.

Several researchers have investigated the performance of semi-rigid steel connections under experimental static cyclic loads. However, earlier research has not surprisingly addressed the existing TA–SP connection behaviours. In order to achieve precise results, it is imperative to conduct comprehensive experimental tests. However, these tests come with challenges, as they are both financially demanding and require a significant investment of time. Alternatively, a more attractive method involving a nonlinear finite element (FE) model can be employed. This model integrates curve-fitting parameters to determine the connection's strength, stiffness, and ductility values. A primary concern is the accuracy of the geometric and model variable expressions, which remain valid only within the limited data range used. This limitation poses safety concerns, especially when the necessary data is not available. The results may also be subject to uncertainties, leading to significant errors in the analysis. These uncertainties, related to the model and geometric properties, play a crucial role, particularly in analysing reliability methods [4].

From this perspective, the current investigation utilises various reliable methods to analyse the reliability of the existing TA–SP connection and ascertain the failure probability of the connection under extreme load conditions. The accuracy of the analysis is contingent upon the precision of the percentile error, which delineates the optimal failure probability outcomes.

For this purpose, the methods introduced in this investigation mimic fast seismic advancements that are becoming increasingly important due to the widespread use of TA–SP connections in Australian metropolises. Furthermore, the fundamental principle of the structural reliability concept may pose challenges, as it encompasses the failure probability of the most vulnerable elements in the connection system.

Finally, the charge is closely tied to the overall TA–SP connection cross-section, magnifying the probability of system failure. Consequently, a system reliability index becomes the foundation of a novel method that aligns with the essential criteria of the ISO 13822 [5], ISO 2394 [6], and JCSS [7] guidelines.

Investigation Method and Framework

Semi-rigid connections have a significant impact on the dynamic behaviour of steel structures. These connections, often overlooked, play a crucial role in the overall performance of flexibly connected frames, and the establishment of semi-rigid joints has been provided in several national design codes.

The concept of semi-rigid connections is well-documented in various studies in the literature. For instance, studies by Richard and Abbott [8], Kishi and Chen [9], Colson and Louveau [10], Azizinamini et al. [11], Bjorhovde, Colson, and Brozzetti [12], Pekcan, Mander, and Chen [13], Faella et al. [14], and Ahmed et al. [15] have explored this topic. Ad-

ditionally, established methodologies are clearly outlined in AISC 360-10 [2] and Eurocode 3 Parts 1–8 [3], allowing for the consideration of semi-rigid connection behaviours that reflect their ranking in terms of the connection classification.

However, the current investigation focuses on assessing the strength of existing TA–SP connections when withstanding extreme loads. The study extends an initial evaluation involving numerical and analytical analysis of the TA–SP connection system. A TA–SP connection prototype was developed, and each connected element was bolted and riveted through the corresponding beam and column flange.

The top angle was initially designed to combine the shear and axial forces in the beam member and was used to increase the lever arm of the bolt group under tension to increase the load-carrying capacity. Such arrangements of the existing TA–SP connection elevations used in the beam-to-column joint are illustrated in Figure 1.

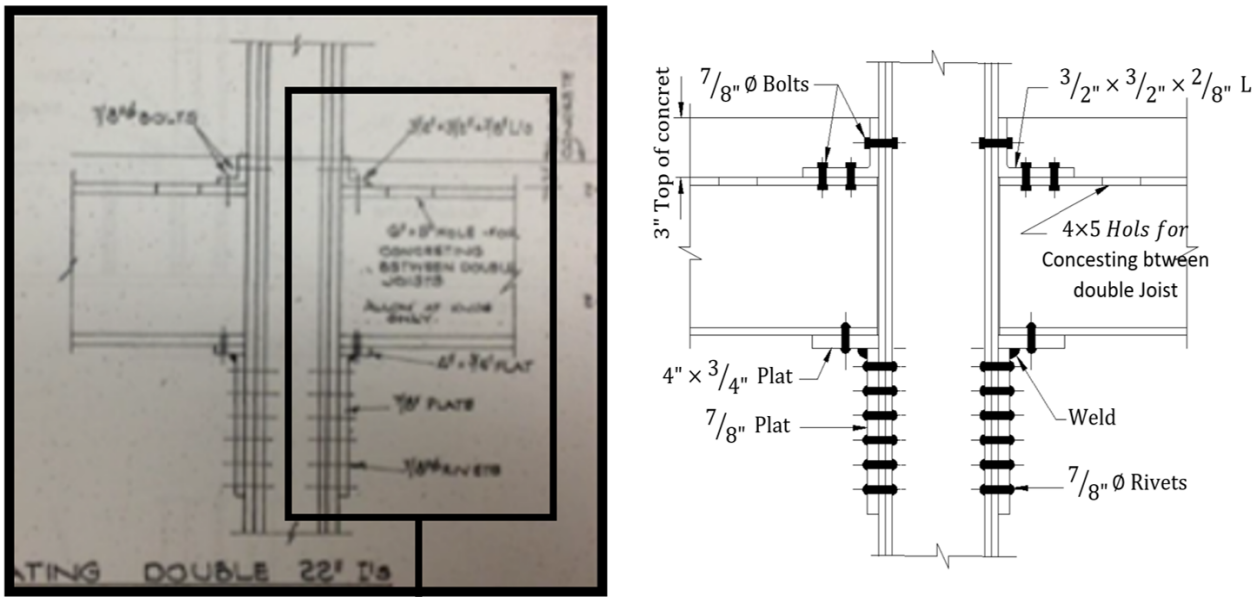


Figure 1. Existing TA–SP semi-rigid connection: (**a**) represents a typical 1920s–1960s semi-rigid connection used in the Australian CBD, and (**b**) replicates the existing TA–SP connection.

Figure 1a,b illustrate the actual connection descriptions, and Figure 2 provides the proposed beam-to-column prototype of the existing TA–SP connection description.

Figure 2 likely refers to a visual representation of the existing connection model. The description of this model includes the following: t_P is an accessory plate 10 mm; t_t top angle thickness 12.7 mm; t_{f1} top beam flange 21.2 mm; h is the beam depth between the top and bottom flange 558.8 mm; t_{f2} bottom beam flange 21.2 mm; t_{Hs} horizontal seat pad plate thickness of 19.1 mm; W_h weld depth 4.36 mm; L_{Hs} length of horizontal seat pad plate 100 mm; t_{VS} vertical plate thickness of 22.2 mm; t_{V1} rivet fasteners spacing 50 mm; h_c is the column full-depth 254.0 mm. The general geometrical parameters of the existing connection prototype are outlined in Table 1.

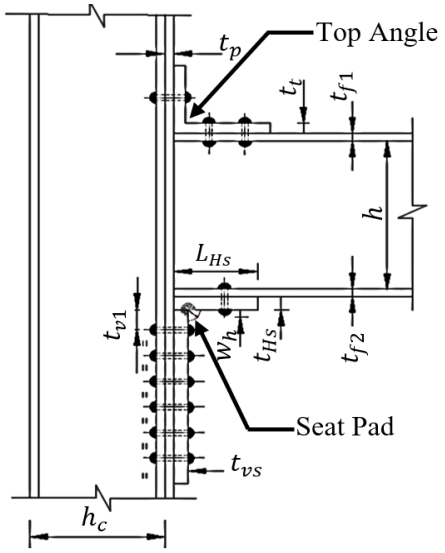


Figure 2. Existing TA–SP semi-rigid connection prototype.

Table 1. Geometrical parameters of the existing connection prototype.

Connections Elements	Specifications for the 1920s to the 1960s Class Steel Members
Beam	$22'' \times 7'' \times 75'$—1920–60 steel product beam member
Column	$10'' \times 8'' \times 55'$—1920–60 steel product column member
Top angle	152.4 mm × 101.6 mm × 12.7 mm
Seat pad	100 (*Hs*) mm × 19.1 mm + 350 (*Vs*) mm × 22.23 mm
Bolt ∅	22.0 mm
Rivet ∅	22.0 mm
Accessory plate	10.0 mm

Accurate analysis of the existing connection can be challenging due to the numerous components and their inherited nonlinear interactions. Its geometrical configurations and specific sections, including the top angle, bolts, rivets, beam, welds, column, and seat pad, significantly influence its system performance. From this perspective, the deductions drawn from this inquiry are as follows:

- The TA–SP connection moment–rotation behaviour prototype will offer valuable insight into its ability to dissipate energy during seismic events.
- The nonlinear FE method analysis reveals the TA–SP connection's inherent ultimate moment capacity (*Mu*).

This comprehensive analysis examines the behaviour of the existing connections, given their practical implications. Although the advantages of traditional semi-rigid connections are well documented, assessing the existing connections remains a subject of ongoing contention. However, given the limited information available, assessing the reliability of the existing TA–SP connections while accounting for potential risks associated with overlooking any impacts remains essential. The evaluation mainly involves exploring a comprehensive framework through a systematic strategy. Specifically, it focuses on system reliability analysis by examining the weakest elements in the connection system, an aspect not previously explored by researchers. In order to gain more insight into the method proposed, Figure 3 illustrates its sequential steps and systematic algorithm introduced in the current investigation.

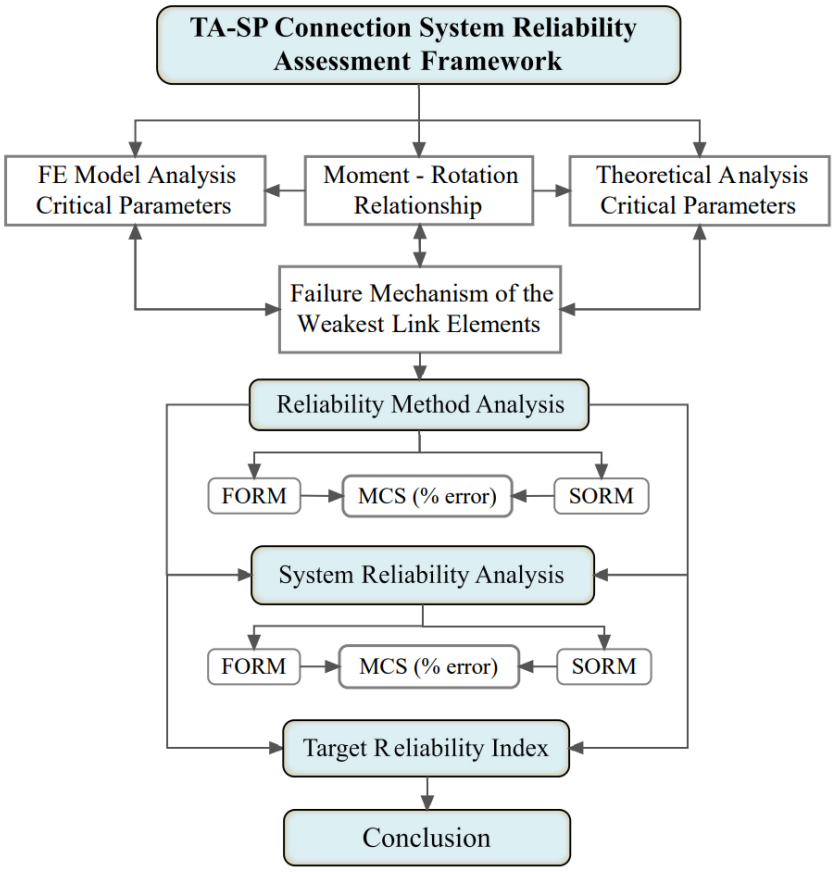


Figure 3. Flowchart of the proposed investigation method framework.

2. Modelling the TA–SP Connection Using the FE Method

The initial stages of the current investigation involve validating the previous research work conducted by Pirmoz and Danesh [16], first and followed by Smitha and Babu [17], samples using ANSYS, the finite element (FE) analysis software. Their study emphasised the importance of the moment–rotation behaviour of the top and seat angle (T-SA) semi-rigid connections, and their outcomes were compared with the ABAQUS [18] FE analysis software model developed in the present investigation. Consequently, the existing TA–SP connection prototype, which shared similar properties and dimensions, was incorporated with validations. While a direct comparison between these analyses lies beyond the current investigation's scope, cross-referencing the authors' other work can help to avoid redundancy [19].

Subsequently, the model incorporates fewer elements, including those composed solely of shell elements. Different mesh sizes arrangements were employed to model the bolts, rivet fasteners, top angle, beam, column, and set pad.

The existing steel material exhibited a yield strength (f_y) of 158 MPa and an ultimate tensile strength (f_u) of 435 MPa, and a 0.2% post-yield stiffness ratio was applied. Each connected component was modelled as a nonlinear element with stress distribution. The applied load at 1500 mm beam length is transmitted to the beam-end via the top angles, bolts, column, rivet fasteners, and seat pad components. The model arrangements are visually represented in Figure 4, which illustrates a 3D model of the TA–SP connection.

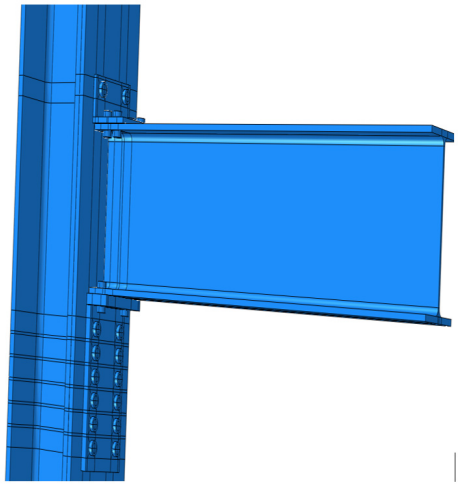


Figure 4. The existing TA–SP connection in the 3D FE model.

2.1. Analysis Results

During the initial stages of this investigation, the number of independent contact interfaces was carefully considered to ensure suitable interaction between the connected element portions. Contact–friction interfaces enabled the simulation of the contact between each element and the surrounding parts.

In test 1, the capacity was limited to 56.7 kNm due to the top-angle capacity. At this loading, the transition was expected to have stresses on the order of 386.1 N/mm^2. This agreed with the FE model, which indicated significant stress as the load increased and the tension stresses reached 515 N/mm^2 in element E2.

In test 2, the theoretical capacity is limited by element E7 and the failure moment of 120 kNm, which had a compression stress of 472.1 N/mm^2. At this point, the weld section is overstressed by 61%, ultimately leading to failure. Figure 5 illustrates the von Mises stress [20] contours at a load close to the test bending under the clockwise rotational failure mechanism of the existing TA–SP connection.

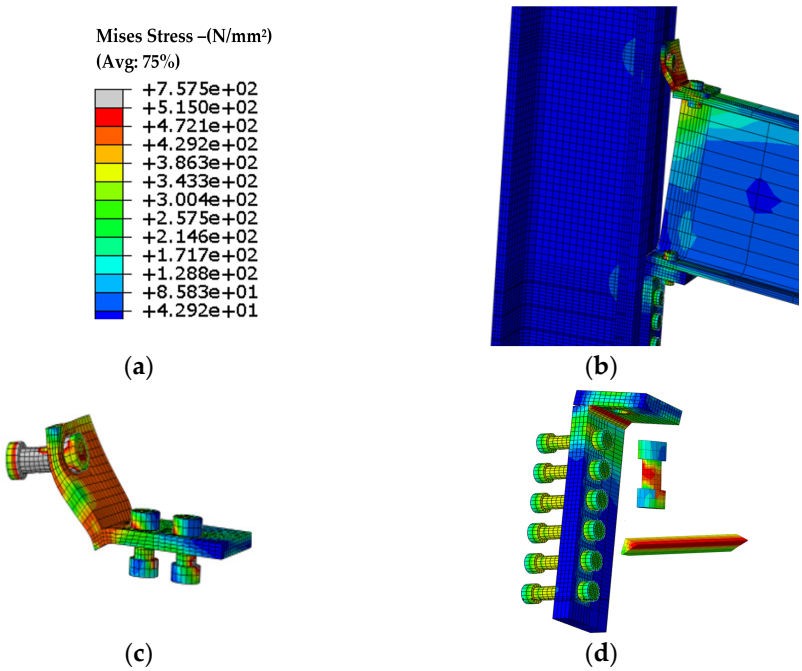


Figure 5. Deformed shapes and stress contour: (**a**) stress values, (**b**) represents the FEM of the TA–SP connection under ultimate load, (**c**) FEM sample element (E2), (**d**) FEM sample element (E7).

The pre-tension force was applied due to a thermal gradient on the bolt's yield. Since there is no information about the amount of bolt pre-tension to be considered, the values of the pre-tension force described by ANSI/AISC 360-10 [21] were applied. A 178 kN pre-tension force was used for a 22.3 mm diameter bolt and rivet fastener at the initial loading stage. Each element was modelled based on a plastic-borne approach, and zero nonlinear rotations were placed to simulate the formation of hinges in the weakest elements. These formations can also relate to the connection moment—rotation relationship and regulate the curve parameters mode.

2.2. Ultimate Moment Capacity of the TA–SP Connection

The existing TA–SP connection system transmits a tensile force into individual elements. For example, Figure 6 illustrates the series system representing the individual elements in the connection system.

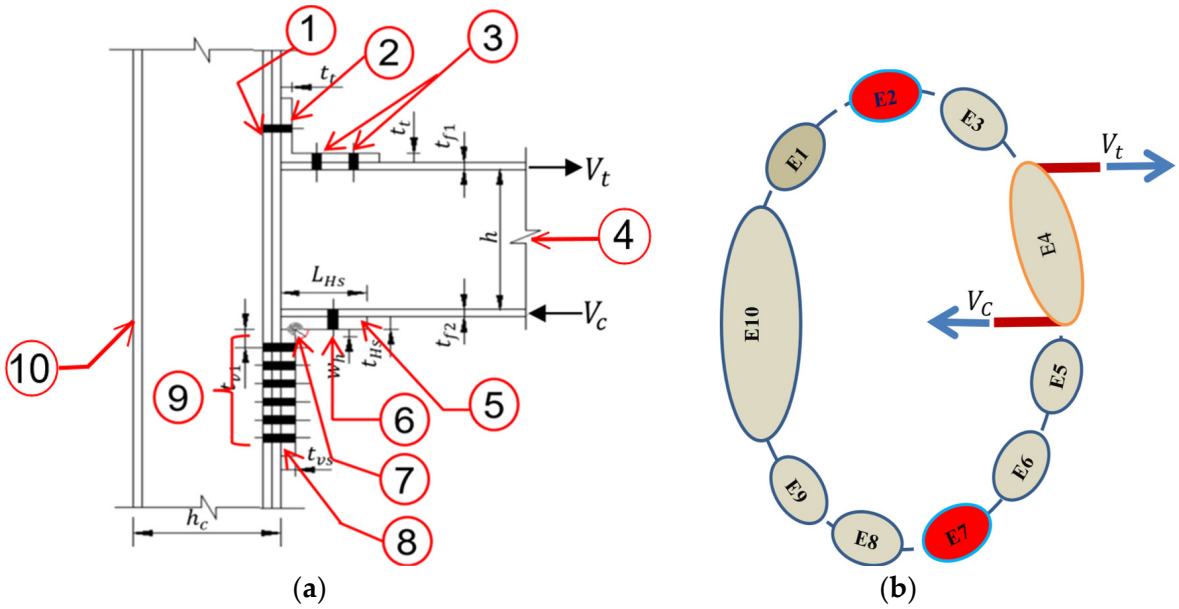


Figure 6. The TA–SP connection system: (**a**) represents the number of 'elements' in the connection system; (**b**) displays the weakest "elements" E2 and E7 in the locked-chain series system mode.

Figures 6 and 7 illustrate that the red block elements E2 and E7 represent the weakest elements in the system. This could continue through many levels of detail, down to the level of the most vital subsystem. Unlike their counterparts, elements E3 and E9 operate parallel subsystems, demanding separate assessments. However, the task of assessing parallel systems is intricate and exceptional. Despite this, E3 and E9 are limited to minor functions and maintain a sequential arrangement.

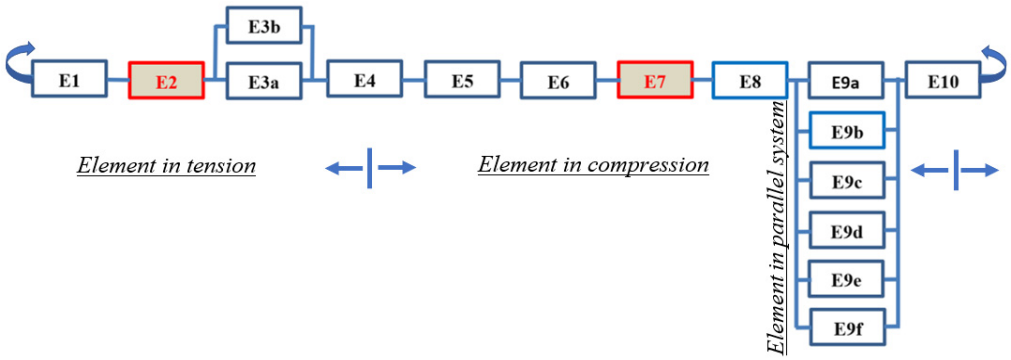


Figure 7. TA–SP semi-rigid connection in chain series system configurations.

The failure of the connection system depends on the strength of its weakest element. Therefore, the Drucker yield criterion [22] is crucial for assessing the maximum tensile force (V_{t1}) in the system. Notably, the prying force (Q_1) in "elements" E1 and E3 plays a crucial role, led by the applied tension forces (V_{t1}), thereby, the geometrical and strength effects in element E2. Therefore, Tresca's yield criterion [23] is pivotal in incorporating the strength limit state, and the limit state equation for the weak element E2 can be given by

$$g(X)_{E2} \approx \frac{f_y b t_t^2}{4} \geq g_1 \frac{V_{t1}}{2}. \quad (1)$$

where g_1 is the gauge length and V_{t1} is the applied tensile force derived from the prying force Q_1 (see Figure 8). Thus, the limit state condition for the element E7 is given by

$$(X)_{E7} \approx V^*_{Res} \geq \varnothing V_W, \quad (2)$$

where $V^*_{Res} \approx \sqrt{(V^*_X)^2 + (V^*_Y)^2 + (V^*_Z)^2}$, $V^*_X \approx 0, V^*_Y \approx \frac{f_y}{2L_w}$, $V^*_Z \approx \frac{V_{c1}}{2b'} \pm \frac{M^*_X \pm \frac{T_d}{2}}{b' \frac{T_d}{2}}$

where M^*_X, is the applied moment by taking a moment at the centre of rotation. Figure 8 illustrates a clockwise rotational mechanism allowing the underlying concepts.

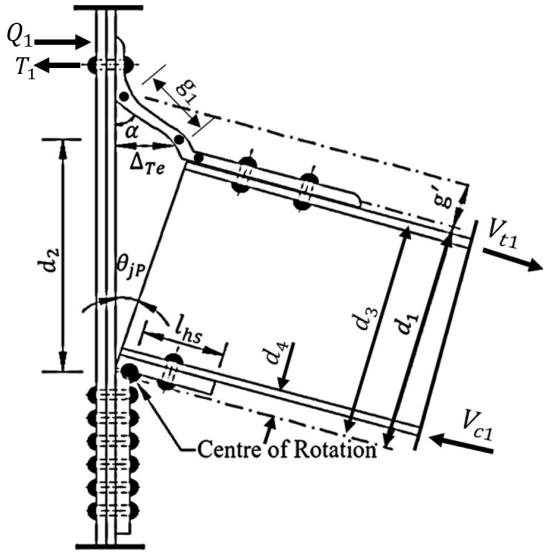


Figure 8. Clockwise rotational failure mechanism of the existing TA–SP connection.

Therefore, the applied moment at the centre of rotation can be defined by

$$M^*_X \approx (V_{t1} d_3 - V_{c1} d_4), \quad (3)$$

where V_{c1} and V_{t1} are the applied tensile and compressive forces, and d_3 and d_4 are a distance from the centre of rotation; thus, the limit state function of the welding capacity is given by the Australian Standard (AS 4100) [24]:

$$\varnothing V_W \approx 0.6 f_{uw} (T_d + 1.5 \text{ mm}), \quad (4)$$

where T_d represents the depth of the weld throat and f_{uw} signifies the strength of the weld. However, the ultimate moment capacity of the existing TA–SP connection can be calculated by taking a moment at the centre of the weld throat.

$$M_u \approx \frac{g_1 V_{t1}}{2} - (V_{t1}\, d_3 - V_{c1}\, d_4) + \frac{0.6 b' (T_d)^2}{4} f_y, \quad (5)$$

It is essential to note that the moment–rotation relationships can be effectively expressed in a self-contained format, enabling easy reference to Equation (5). Therefore, the parameters, such as the initial stiffness, ultimate moment, and rotational capacity, can be cross-referenced in the authors' other work to avoid duplication [19].

2.3. Validation

To facilitate the practical application of nonlinear FE method analysis, the precise moment–rotation curve includes essential parameters like the initial stiffness (*Rki*), ultimate moment resistance (*Mu*), and shape parameter (*n*) at different curve levels, enabling a more profound consideration of the weakest element's effect. It also highlights the critical parameter mode of the existing TA–SP connection, offering valuable insights into the behaviours of the TA–SP connection, as shown in Figure 9.

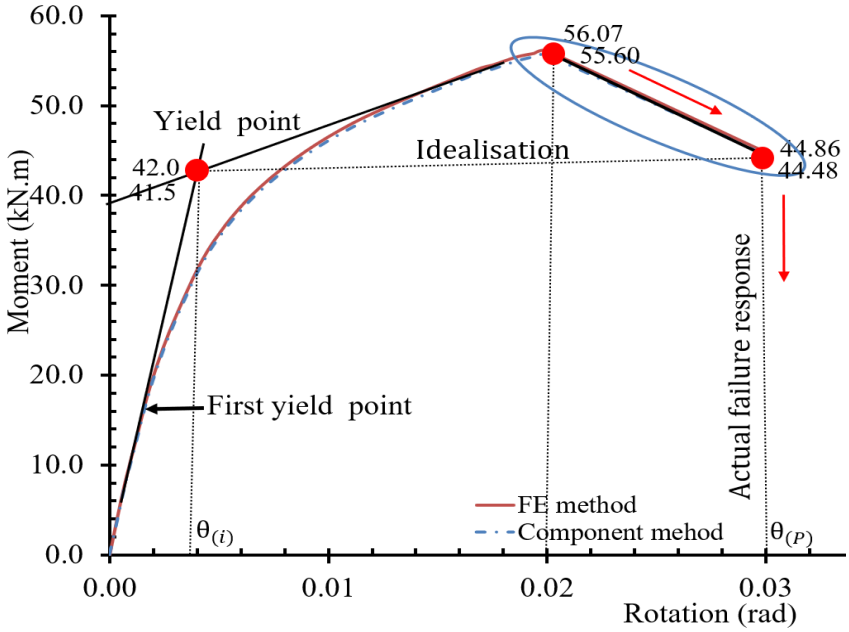


Figure 9. Comparison of the moment–rotation curve parameters of the TA–SP connection.

The analysis indicates an elastic-to-plastic transition occurring at increments of 0.01 rotation. According to ANSI/AISC 360-10 guidelines [21], the rotational limit for ultimate resistance is set at 0.02 radians. The plastic resistance rotation accounts for stiffness degradation during a cycle of up to 0.03 radians; this behaviour is evident from this study's moment–rotation relationship curve. This result was also compared with analytically predicted values, and the results of the FE method are slightly superior to the analytically predicted values. However, both methods demonstrated relatively close results and effectively captured the behaviour of the TA–SP connection parameters.

3. Analysing the Failure Mechanisms of the Weakest Elements in the System

In previous assessments, a critical unknown parameter related to the required toughness level in the section was the stress distribution that emerges at the beam-column interface due to the applied top angle and beam rotation. The uniform yield stress across the top angle thickness results in conservative toughness estimates. However, the critical unknown factor remains the distribution of applied and residual stress between the outer surface of the column and the beam flange region, illustrated in Figure 5.

The FE model of the TA–SP connection indicates a significant progression in understanding the required toughness. The estimation of toughness exceeds the scope of this investigation; however, the model is strategically applied to the weakest element of the connections, necessitating a thorough analysis. Following standard practice, the top angle

executes a plastic moment conveyed to the model via tensile force testing. As per the usual convention, the weld is overmatched compared to the vertical and horizontal seat pad elements. Therefore, a normalised moment distribution was developed by combining the applied and resisting moment values at the most critical location. Considering the beam rotation functions, this allowed through-thickness and gauge length change expression at the top angle.

For the different levels of plastic rotation (between 0.02 and 0.03 radians), the moment distribution at the three most plastic hinge locations was normalised, considering the top-angle plastic yield. It is then considered a function of the top angle leg, expressed by the gauge length up to a maximum of 31 mm. The resultant plots from the analysis, which show the applied and resistance moment versus the deformed gauge length, are a beam rotation function. Their most significant effect is the increase in elasticity up to a limit of 0.02 radians of rotation. Beyond this point, the capacity diminishes with increasing rotations. These actions encompass the failure mechanisms of elements E2 and, eventually, E7. Therefore, their performance is closely related to the full range of beam rotation in hysteretic behaviour, as schematically depicted in Figure 10.

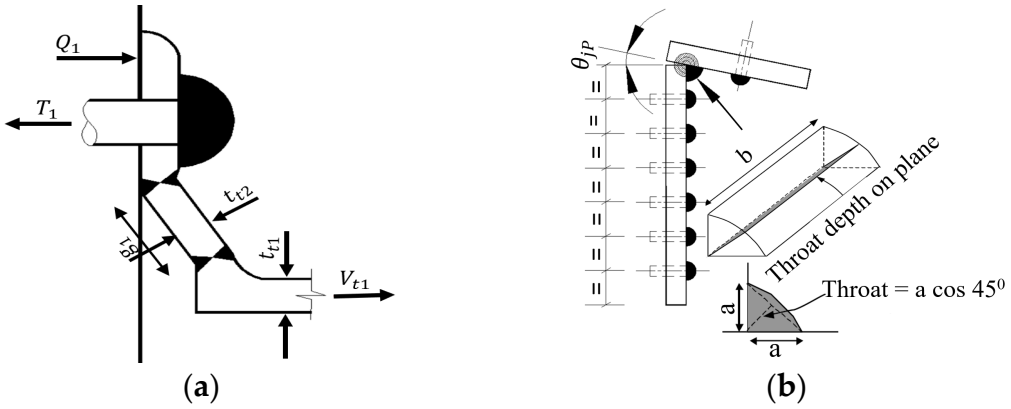


Figure 10. Failure mechanism of the weakest elements: (**a**) element (E2) shows failure mechanism under tensile force, and (**b**) shows "element" (E7) failure behaviours under compressive force.

Both elements exhibit incremental failure processes that vary within the range of 0.0 to 1.0, influenced by the proportional load factor (φ_n). Additionally, the beam rotation is restricted to a range between 0.02 and 0.03 radians, and at 0.03 radians, both the applied and resisting moments fall within a defined range, indicating that the connection resistance is no longer sufficient. Figure 11a,b illustrate the analysis results chronologically, comparing the beam rotation under the ultimate and the plastic moment response, signifying the effects of "elements" (E2 and E7) failure and safe states. Both "elements" performances are scrutinised from a limit state point of view, in line with the designated gauge length, until 119.2 kN tensile force is reached to their maximum plastic limits. However, both performances exhibited comparable pre-yield stiffness initially, and their behaviours diverged after reaching their yield point. The analysis results show consistency with the maximum gauge length of 31.5 mm, leading to the maximum yield stiffness at the plastic moment capacity of the existing connection.

To further validate these findings, the subsequent section delves into the probability of failure that influences the overall system reliability directory.

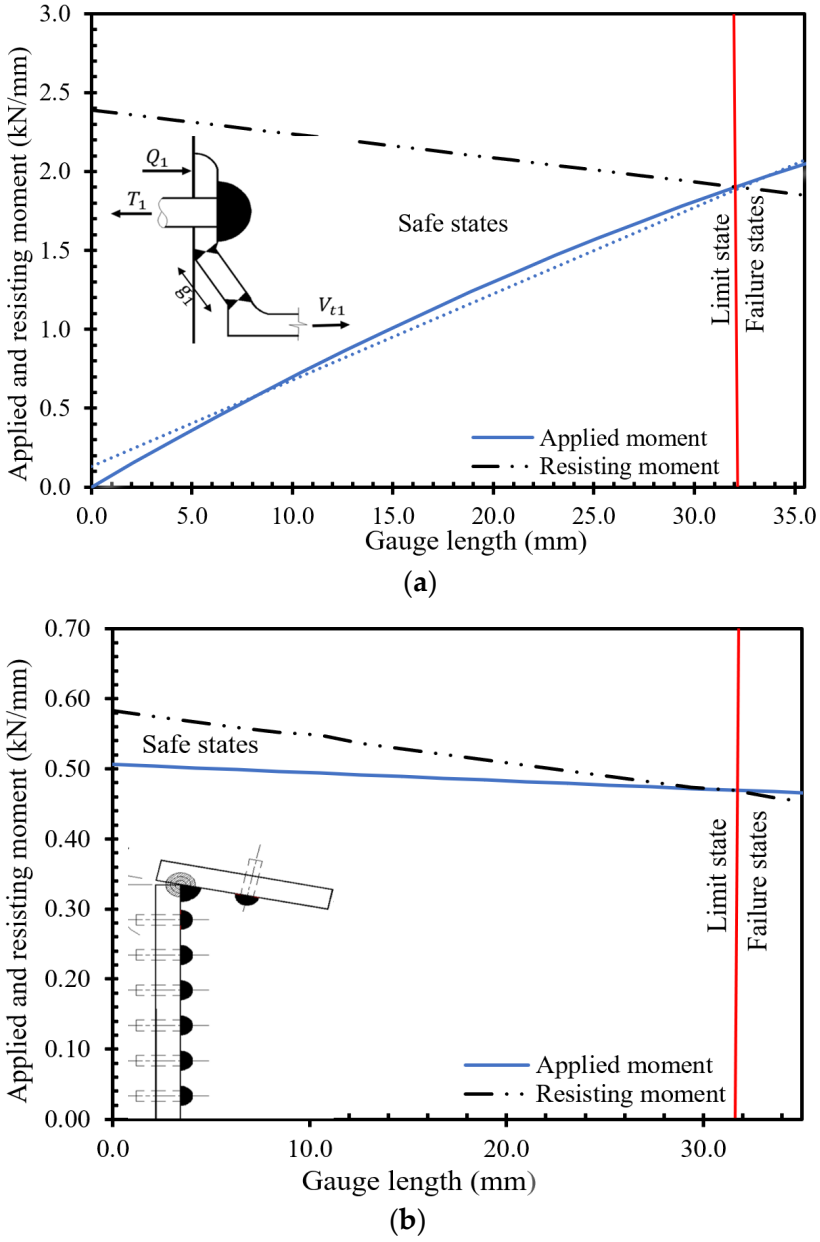


Figure 11. Applied (M^*) and resisting moments (Mr) Vs the gauge length (g_1): (**a**) represents failure and safe states of "element" E2; (**b**) represents failure and safe states of "element" E7.

4. Data Inputs for Deterministic Analysis

In the context of failure-mechanism-based analysis, the principal factors to consider are the applied and resistance moments. Specifically, when evaluating the weakest elements (E2 and E7) in the connection system, each input variable is depicted on the assessment diagrams, as shown in Figure 11a,b. The diagram serves as a visual aid that indicates the analysis arguments, whether they fall within a safe or failure state. This deterministic analysis requires the seat of the worst-case scenario at the plastic moment resistance assumption inputs, and their results are correspondingly conservative. It is, therefore, crucial to assess both elements' responses according to their properties' variations.

To account for uncertainties in the applied moments, we assigned an incremental interval equal to 0.7 times the maximum tensile force value of 119.2 kN. This interval between the upper and lower bounds corresponds to positive and negative multipliers; thus, the limits reflect the uncertainty.

In this instance, the applied and resistance moments are random variables, and thus, reference to material properties from the relevant database enables realistic distributions that are likely to define the weakest "elements" resistance parameters. The integral functions of these parameters represent a mean and standard division, and each variable possesses a statistical distribution that factors the uncertainty. The probability distribution relies on the statistical properties of the random variables drawn from practical recommendations by JCSS [7], Ellingwood [25], Fisher and Galambos [26], Galambos and Ravindra [27], and Kennedy and Gad Aly [28]. The section properties are sourced from Melcher et al. [29] and Holicky and Sykora [30]. Additionally, past research provided data on existing steel products (1923-A3, 1936-A36, 1955-A36, and 1963-A36) with strengths of 124, 138, 158, and 158 MPa [25]. Further, Ellingwood provides formulas for determining the existing steel-type yield strength, such as $0.95(fy - 4\ ksi)$ or $0.95(fy - 28\ \mathrm{N/mm^2})$ [25]. These variables are specifically related to the existing TA–SP connection, as outlined in Table 2.

Table 2. Statistical variables and probability distributions.

Variables	Symbol	Distribution	E [−]	CoV
Section model	Zx	Normal	1.00	0.05
Thickness	t	Normal	0.964	0.039 0.025
Yield stress	f_y	Log-normal	1.05	0.110
Fillet weld	w_n	Log-normal	0.84	0.150
Height and width	$h\&w$	Normal	1.00	0.002

The shear weld strength ratio is 0.88, with a coefficient of variation (CoV) of 0.11. If weld fabrication is involved, a 0.15 CoV is recommended [26].

4.1. Assessing the Failure Probability of the TA–SP Connection System

The existing connection operates on a statically determined basis, rendering it susceptible to system failures. Its vulnerability arises from the possibility of plastic hinges forming in any of its elements. The formation of a hinge within the system triggers failures and makes each element susceptible to failure modes. Therefore, the probability of system failure depends on the weakest link among the n-th elements, as earlier quoted by Freudenthal [31]:

$$P_f \approx P(E_1 \cup E_2 \ldots\ldots\ldots\ldots \cup E_n), \tag{6}$$

where E_i is the event of failure in the i-th element mode $(i = 1, 2, 3 \ldots n)$. Hence, the probability of system failure can be expressed as follows:

$$P_f \approx P[\mathrm{g}(X) \leq 0] \approx \int \ldots \int f_x(x) \partial_x, \tag{7}$$

where $f_x(x)$ is a density function of joint probability; in this case, the limit state function is given by $\mathrm{g}(X) = 0$, where X is a vector of random variables and can be expressed by the relationship between the applied force, X_F, and the resistance elements X_R. If $\mathrm{g}(X) \geq 0$, the limit state event is considered safe, and if $\mathrm{g}(X) < 0$, it falls into the failure set. Consequently, this condition can be expressed by the limit state equation as follows:

$$\mathrm{g}(X) \approx F(X_{Ri}) - F(X_{Fi}), \tag{8}$$

where F_i is a function of the shear force in the i-th element, and R_i, denotes the resistance of the i-th element. With such a perspective, the Weibull expression gives the cumulative distribution function $(F_{Ri}(r))$ of the i-th strength [32]:

$$F_{Ri}(r) \approx P(R_i \leq r_i) \approx 1 - P(R_i > r_i)$$
$$F_{Ri}(r) \approx 1 - P(R_1 > r_1 \cap R_2 > r_2 \cap \ldots \cap R_m > r_m),$$

For individual elements, the strength is then expressed as follows:

$$F_{Ri}(r) \approx P(R_i \leq r_i) \approx 1 - [1 - F_{R1}(r_1)] \ldots [\, 1 - F_{Rm}(r_m)],$$
$$F_{Ri}(r) \approx 1 - \prod_{i=1}^{m} [1 - F_{Rn}(r_n)], \quad (9)$$

4.2. Analysing the TA–SP Connection through a Locked-Chain System

The principle of the existing TA–SP connection is an intricate assembly of interconnected and equally dependent mechanisms. The operational state of this system is governed by specific conditions, with each element capable of exhibiting either a functional or failure state. In the event of a failure in one element, the structural integrity of the remaining elements is compromised, potentially triggering a brittle failure. This state could result in low statistical determinations, instigating a systemic issue. To illustrate this concept, consider Figure 6b, which depicts a locked-chain series system composed of ten independent elements, emphasising their critical role in diverse functional modes.

In this particular configuration case, the system may experience failure due to the tensile forces exerted by the clockwise rotational failure mechanism. In order to illustrate this phenomenon accurately, it is essential to formulate a corresponding model of the weakest element failure event (En), where $En = \{Xi > Si$ expresses the failure event$\}$ and X_i, is the applied force $X_{F,}$ distribution among the elements, Si is a function of the resistance X_R for the distributed strength of the interconnected elements, and i represents each connected element (for example, $i = 1, 2, \ldots n$) facing a failure event. Consequently, the failure probability of the union events can be resolute by rearranging Equation (6).

$$P_f \approx \sum_{n=1}^{i=n} P_{f1} \cup P_{f2} \ldots \cup P_{fn}. \quad (10)$$

However, the fundamental case is generalising with several correlations to the uncertainty of the "variables". Such correlations must be formulated to ensure that the reliability of the existing connection applies to the limit state.

5. Structural Reliability Approaches

This study introduces the use of structural reliability to evaluate the TA–SP connection system. It discusses commonly used techniques like FORM [33] and SORM [34] to simplify calculations and determine the reliability index. The Monte Carlo simulation (MCS) [35] was introduced to compare the accuracy of the results. Meanwhile, advanced computational tools like Mathcad 15 [36] and spreadsheets were employed to streamline the simulations.

5.1. First-Order Reliability Method

The first-order reliability method aims to represent uncorrelated random variables in a linear limit state function utilising the first and second moments [37]. The method includes the first-order second-moment (FOSM) and the advanced first-order second-moment (AFOSM) approach. The FOSM method ignores information about the distribution of random variables. On the other hand, the distribution of random variables is aptly utilised in AFOSM.

5.1.1. Estimating the Probability of Failure Using FOSM

The clockwise rotational mechanism of the existing connection represents an optimal scenario for plastic failure, delineating the minimum reliability of its weakest elements. The connection system is deterministic and distributes the tensile force equally among

elements despite variations in strength and size. The FOSM approximation is ideal but encounters limitations due to the first-order Taylor expansion for managing the nonlinear limit state functions. Thus, the failure probability of the weakest element can be estimated by substituting Equations (6) and (9) into Equation (11).

$$P_{fi} \approx F_V(V_t) \approx \Phi(-\beta_2)_{E2},\ for\ E7 \approx \Phi(-\beta_7)_{E7}, \tag{11}$$

Consequently, it can be simplified as

$$P_f \approx \Phi\left(\frac{(R_i) - \varphi_n(S_i)}{\sqrt{\sigma_{Ri}^2 + \sigma_{Si}^2}}\right)_{E2} \cup \Phi\left(\frac{(R_i) - \varphi_n(S_i)}{\sqrt{\sigma_{Ri}^2 + \sigma_{Si}^2}}\right)_{E7}, \tag{12}$$

The resistance and the applied load are modelled using the Gaussian distribution N(μSi, σSi) for the mean and standard deviations value of the applied moment for the i-th element and N(μRi, σRi) for the mean and standard deviations value of the resistance for the same element. Consequently, the equation for calculating the reliability index for the i-th element can be given through the negative of the inverse cumulative distribution function (CDF) of the standard normal distribution [38]:

$$\beta_{FORM} \approx \Phi^{-1}\Big(P_f\Big), \tag{13}$$

5.1.2. Estimating the Probability of Failure Using AFOSM

The advanced first-order second-moment method involves transitioning the reduced variable to the standardised coordinate system [37]. Consequently, the reduced random variable can be expressed as follows:

$$X_i' \approx \frac{X_i - \mu_{xi}}{\sigma_{xi}}, \tag{14}$$

where i designates $E_1, E_2 \ldots E_{10}$ of the limit state function of the component, as referred to in Equation (3) and can be rewritten as $g\left(X_1', X_2' \ldots X_n'\right) \approx 0$. This represents the minimum vector distance point from the origin of x* and simplifies the random variables of $(X_1, X_2 \ldots X_n)$ at the design point. However, for a more refined analysis of consistent coordination, the Hasofer–Lind reliability index [39] can be used to determine the minimum vector distance point from the limit state surface:

$$\beta_{HL} \approx \sqrt{(x'^*)^T (x'^*)}, \tag{15}$$

It also represents the minimum random variables of the load-carrying capacity (R_i'), and the applied moment (S_i'). Both variables are independent and expressed by the Gaussian random variables N(μ_{ri}, $\sigma_{X_{ri}}$) and N(μ_{mi}, $\sigma_{X_{mi}}$):

$$R_i' \approx \frac{R_i - \mu_{ri}}{\sigma_{X_{ri}}}, \qquad S_i' \approx \frac{S_i - \mu_{mi}}{\sigma_{X_{mi}}}, \tag{16}$$

From this perspective, the limit state function can be driven by

$$Z_i \approx \sigma_{X_{ri}} R_i' - \sigma_{X_{mi}} S_i' + \mu_{ri} - \mu_{mi} \approx 0, \tag{17}$$

where Z_i is a Gaussian distribution comprising the chain rules. As such, the partial derivative of the performance function at the design point of the origin is given as follows:

$$\frac{\partial_g}{\partial_{f_y}}\bigg|_{\partial X_i^*} \Big(\sigma_{fy}\Big)_i; \qquad \frac{\partial_g}{\partial_{z_p}}\bigg|_{\partial X_i^*} \Big(\sigma_{z_{pI}}\Big)_i, \tag{18}$$

Then, the reduced design point $(n-1)$ of the variable is expressed by

$$f^*_{y1} \approx \left(\mu_{fy} + \sigma_{fy}\beta\alpha_{fy}\right)_i \quad Z^*{}_1 = (\mu_z + \sigma_Z\beta\alpha_Z)_i, \tag{19}$$

where α_n is a direction cosine at the minimum distance point of x^*_i, which can be articulated by the following equation [40]:

$$\alpha_{fy} \approx \left(\frac{-\sigma_{fy}f^*_y}{\sqrt{\left(\sigma_{fy}fy^*\right)^2 + (\sigma_Z Z^*)^2}}\right)_i, \alpha_Z \approx \left(\frac{-\sigma_Z f^*_y}{\sqrt{\left(\sigma_{fy}Z^*\right)^2 + (\sigma_Z fy^*)^2}}\right)_i, \tag{20}$$

Hence, the normalised value of the design point at the origin space is given by

$$x^*{}_i \approx \left(\beta^2\alpha_Z\alpha_{fy} + \beta\alpha_Z + \mu_{fy}\mu_z\right)_i, \tag{21}$$

Accordingly, Figure 12 illustrates the uncorrelated minimum-distance point at the limit state surface for elements E2 and E7.

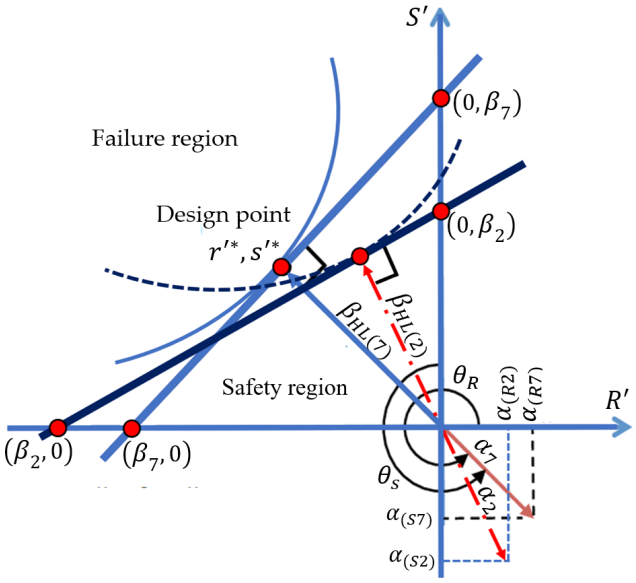


Figure 12. Uncorrelated Element E2 and E7 coordinates at a minimum distance from the origin.

Here, r'^* and s'^* denote the design points at the limit state surface, reflecting the reduced reliability index. Accordingly, Table 3 elucidates this convergence, observed at the third iteration cycle, indicating their corresponding failure probabilities.

Table 3. Summary of the iterative cycle.

Iteration Cycle No.	Element E2		Element E7	
	β_{HL}	P_f	β_{HL}	P_f
1	−3.098	9.73×10^{-4}	−3.199	6.89×10^{-4}
2	−3.080	4.26×10^{-3}	−3.198	6.93×10^{-4}
3	−3.080	1.04×10^{-3}	−3.198	6.93×10^{-4}

5.2. Estimating the Probability of Failure Using SORM

The second-order reliability method (SORM) is used for reliability analysis that considers second-order effects. It provides a more accurate estimation of the reliability index by

considering the nonlinearity of the limit state function and the non-normal distribution of input variables on the limit state surface [33]. The SORM is a robust method that quickly delivers reliable results using the first-order reliability method (FORM). The method involves Rosenblatt transformation [41], which converts random variables X_i, to a non-normal distribution in the limit state surface. The conversion of the random variables X_i to standard variables Y_i is given by

$$Y_i \approx \frac{X_i - \mu^e_{Xi}}{\sigma^e_{Xi}}, \tag{22}$$

The mean (μ^e_{Xi}) and standard deviation (σ^e_{Xi}) of X_i, for the minimum distance of a design point (x^*_i) are crucial parameters. Identical methodologies can be applied to estimate the equivalent parameters for log-normal X_i. The probability of failure can be calculated using the probabilistic model of g(X_i), representing the cosine direction at the minimum-distance design point [36]. When applied to elements E2 and E7, their random variables are converted to a non-normal distribution. For an illustration of the setting, Figure 13 provides for both non-normal distributions in the limit state surface, which quotes a previous study by Arteaga and Soubra [42].

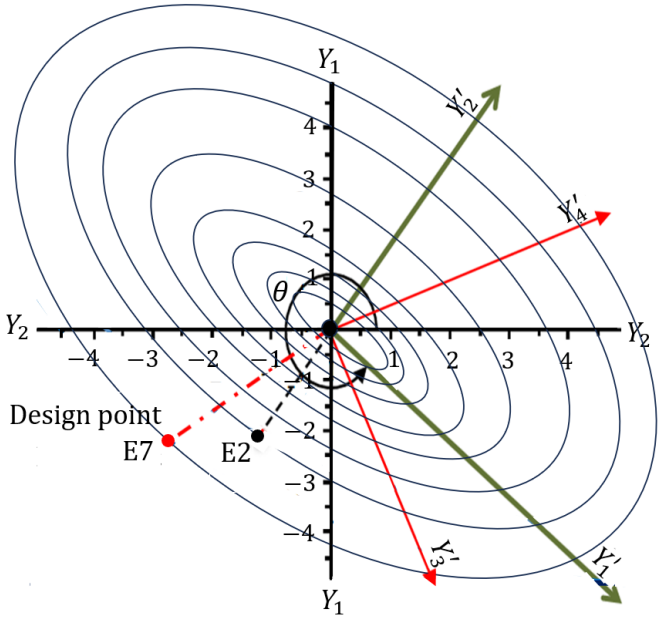


Figure 13. Element E2 and element E7 rotations about the axes on the reduced space.

This process involves the Rosenblatt transformation and a differential operator, where an ($n \times 1$) matrix with differential equations defines the eigenvector function scale. The relationship between the eigenvector function and the decomposed diagonalised matrix encompasses rotational coordination (θ), emphasising the geometric descriptions. Consequently, such expressions emphasise an orthogonal transformation of the rotation matrix B_i, which is accessible from the direction cosines α, orchestrating a component gradient vector units as the equation is illustrated in the following rotation matrix form:

$$B_i \approx \begin{bmatrix} Cos\theta & \cdots & Sin\theta \\ \vdots & \ddots & \vdots \\ -Sin\theta & \cdots & Cos\theta \end{bmatrix}_i, \tag{23}$$

where $\theta = 270^\circ + \tan^{-1}(y^*_2/y^*_1)$, and these expressions can also be represented by the matrix form, given the second-derivative performance function of the chain rule:

$$D_i \approx \left| \begin{matrix} \frac{\partial^2 g}{\partial Y_1^2} & \frac{\partial^2 g}{\partial Y_1 Y_2} \\ \frac{\partial^2 g}{\partial Y_1 Y_2} & \frac{\partial^2 g}{\partial Y_2^2} \end{matrix} \right|_i = \left| \begin{matrix} 0 & x_2^* \sigma_{x1} \\ x_1^* \sigma_{x2} & 0 \end{matrix} \right|_i, \tag{24}$$

where x_i^* is a design point at a minimum distance for the i-th element ranging from -90 to 90 degrees. Thus, the second derivative of the limit state function at the design point is given by the eigenvalues of a matrix A:

$$A_i \approx \left| \begin{matrix} \left[cos\theta + \left(\frac{\partial_g^2}{\partial Y_1^2} \right) + \frac{0.8 cos\theta}{|\nabla G(y_n^*)|} \right] & \left[sin\theta + \left(\frac{\partial_g^2}{\partial Y_1 Y_2} \right) + \frac{0.8 sin\theta}{|\nabla G(y_n^*)|} \right] \\ \left[-sin\theta + \left(\frac{\partial_g^2}{\partial Y_1 Y_2} \right) + \frac{0.8 sin\theta}{|\nabla G(y_n^*)|} \right] & \left[cos\theta + \left(\frac{\partial_g^2}{\partial Y_2^2} \right) + \frac{0.8 cos\theta}{|\nabla G(y_n^*)|} \right] \end{matrix} \right|_i, \tag{25}$$

where i is an individual connection element of (E_1, $E_2 \ldots E_{10}$); thus, the last row and last column are computed for the eigenvalues A_i value. Intrinsically, the second-order probability failure approximation can be given by taking into account the eigenvalue (v_i) value of the matrix A_i [33]:

$$P_{fE2} \approx \left[\Phi(-\beta_2) \prod_{i=1}^{n-1} (1 + \beta_2 v_2)^{-1/2} \right]_{E_2} \cup \left[\Phi(-\beta_7) \prod_{i=1}^{n-1} (1 + \beta_7 v_7)^{-1/2} \right]_{E_7}, \tag{26}$$

where β_2 and β_7 are first-order reliability indexes [31] representing elements E2 and E7. Accordingly, Equation (26) can be transformed into the inverse standard normal distribution function, expressing the reliability index of the weakest elements.

6. Results in Percentile Error

In order to compare the accuracy of the FORM and SORM, ten thousand simulations were performed using a Monte Carlo simulation (MCS) [35], measuring the number of performance functions g(x). Furthermore, a system-reliability-based analysis was used, where the performance function is more efficient in determining the probabilities of failure. As for efficiency, the recent literature highlights the percentile error as a measure of maximisations, comparing the probability of failure. It generally involves a set of numbers that indicate the fractional difference when calculating the probabilistic model [43]. Thus, control of the percentile error is given as follows:

$$Error\ \% \approx \left(\frac{P_f - P_{f_{MCS}}}{P_{f_{MCS}}} \right) \times 100, \tag{27}$$

In this respect, the MCS provides a reference for comparison, and Table 4 presents the calculated probabilities of failure corresponding to the percentile errors, which are also plotted in Figures 14 and 15.

The AFOSM and FOSM approaches tend to overestimate the probability of failure, resulting in lower efficiency compared to the SORM percentile errors. In particular, the SORM method yields approximately 27.1% and 49.7% higher than the AFOSM method and relatively 87.7% and 154.33% higher than the FOSM method for both elements. This difference is expected, as the SORM method considers both first- and second-order effects, capturing the curvature of the performance function.

In comparison, the MCS values are significantly higher than those from the AFOSM method, with an increase of approximately 100.1% and 113.1%. They are also substantially higher than those from the FOSM method, with an increase of 195.6% and 262.1%. The reason for the significant error is that the limit-state function in the X-space is nearly linear. The linearisation in the limit state surface produces a significant error. Despite this difference, they capture a substantial portion of the percentile errors, accounting for 80% and 65.7%.

Table 4. Failure probabilities and percentile errors.

	Top Angle (E2)			Weld (E7)		
Calculation Type	β	P_f	**Error**	β	P_f	**Error**
AFOSM	−3.09	9.99×10^{-4}	100.1%	−2.92	1.74×10^{-3}	113.1%
FOSM	−2.97	1.48×10^{-3}	195.6%	−2.75	2.96×10^{-3}	262.1%
SORM	−3.16	7.86×10^{-4}	57.4%	−3.05	1.16×10^{-4}	42.4%
MCS	−3.29	4.99×10^{-4}		−3.15	8.16×10^{-4}	

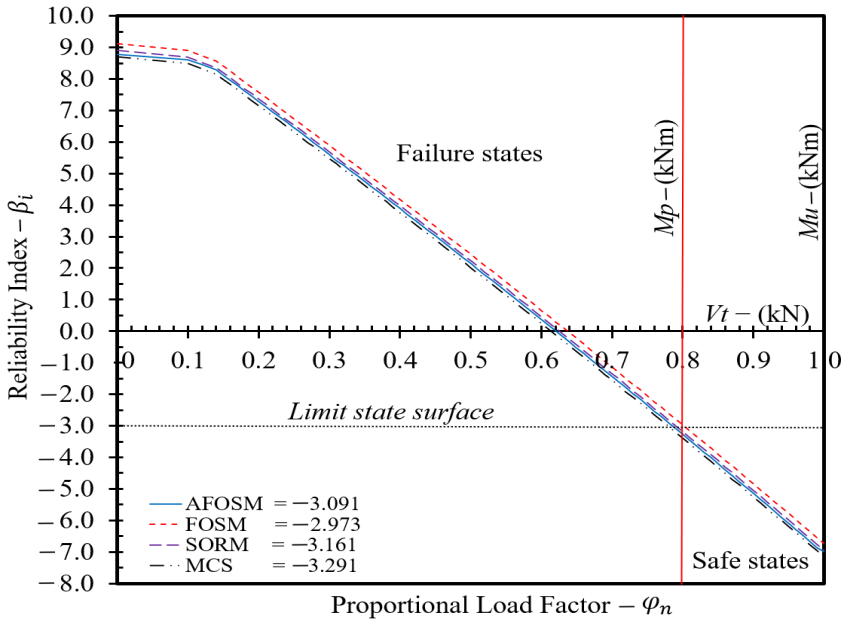


Figure 14. Variation in the reliability index vs. proportional load factor for element E2.

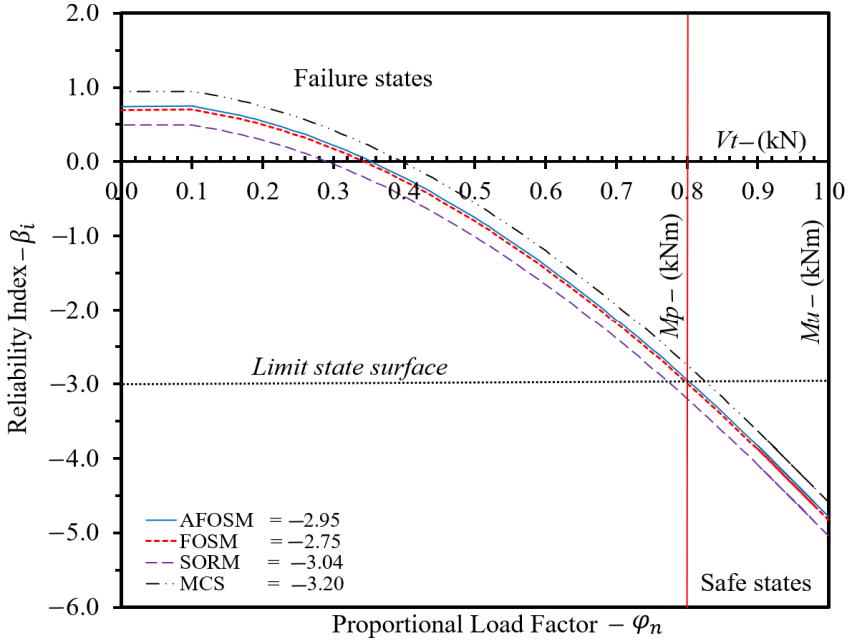


Figure 15. Variation in the reliability index vs. proportional load factor for element E7.

A vital aspect of this study involves the differences between the SORM and the MCS analysis results, and the MCS result exhibits higher values than SORM values. Their differences are approximately 57.4% in E2 and 45.99% in E7, which indicates the MCS has more accurate results due to the 10,000 sample simulation results. However, even though these differences are notable, they are within the same order of magnitude and are not significantly divergent.

The analysis results are presented in Figures 14 and 15. They display that the AFOSM is more accurate than the FOSM, and the SORM is significantly more efficient than the AFOSM in both element analysis cases. As expected, the SORM may not be as accurate as the MCS. The error in E7 appears slightly higher than in E2. The SORM results are generally much more efficient than those of the FORM. However, the applicability of these results can extend beyond their current scope to encompass quadratic functions. Thus far, a single-component reliability analysis has been employed due to the involvement of a singular limit state function. This approach could be extended to a system reliability analysis that illuminates a prospect that warrants further exploration.

7. System Reliability Analysis of the Existing TA–SP Connection

Over the past four decades, extensive research has been conducted to evaluate the reliability of individual structural members, thereby informing design codes. However, when comparing the reliability of single members to that of entire systems, it becomes apparent that system reliability analysis consistently yields higher results due to its advantageous load distribution effects. Various failure modes were considered when assessing each element of the existing TA–SP connection system. Treating it as a parallel system allows it to be conceptualised as a series of parallel systems [44].

The probability of failure mode is then to be the *i*-th element in the system, and ultimately, the *i*-th element arranges the probability of system failure in parallel. Figure 16 provides a graphical representation of a series chain system, illustrating how the probability of system failure can be interrelated and, notably, differs from the physical connections of system failures. These can be assessed in two ways: analytical or simulation computational modes. The analytical mode uses the exact reliability solutions for the system, employing the system's reliability function or the cumulative density function (CDF). In this context, it refers to the reliability analysis that does not need repairs or restoration actions of the existing connection elements. On the contrary, the simulation mode considers repairs or restoration actions, including human risk, behaviours, and additional events outside the context of the present investigation.

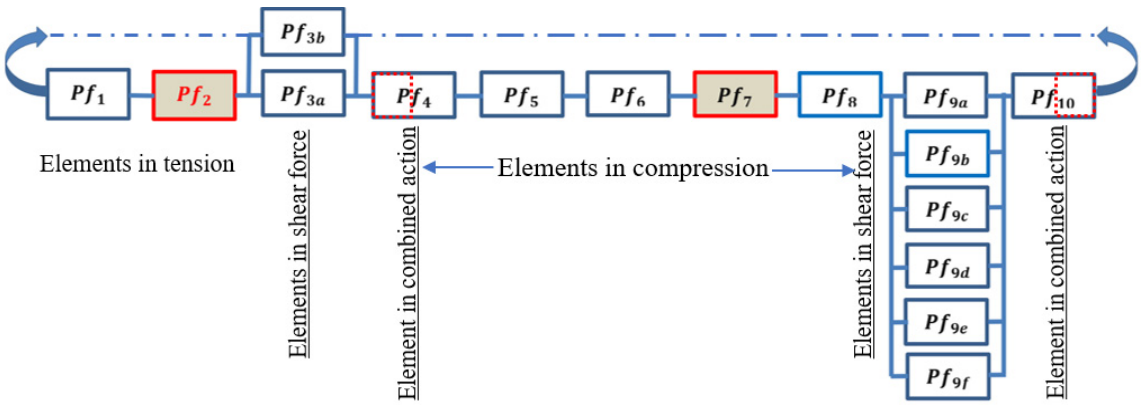


Figure 16. Probability of system failure configuration of the existing TA–SP connection.

However, the analytical approach involves a mathematical expression that describes the system's reliability in terms of its weakest elements. Subsequently, the red boxes shown in Figure 16 represent the most vulnerable components of the series chain system. The probability of system failure can be expressed by rearranging Equation (10).

$$\left(P_f\right)_S \approx \sum_{i=1}^{n} \left(P_f\right)_1 \cup \ldots \left(P_f\right)_2 \ldots \cup \left(P_f\right)_7 \ldots \cup \left(P_f\right)_n, \tag{28}$$

where $i = 2$ and $i = 7$ enclose the relationships among the union of the weakest link events. The performance function of the series system can then be expressed using the inverse standard normal distribution function. This enables the system reliability index to explicitly focus on the weakest element during the clockwise rotational failure mechanism of the existing TA–SP connection.

$$\beta_S \approx -\Phi^{-1}\left[\left(P_f\right)_2 \cup \left(P_f\right)_7\right] \tag{29}$$

The comparison between the system failure probabilities and percentile errors is summarised in Table 5.

Table 5. System failure probabilities and percentile errors.

Calculation Type	P_{fS}	β_S	Error (%)
AFOSM	2.74×10^{-3}	−2.78	108.2
FOSM	4.43×10^{-3}	−2.62	236.8
SORM	1.95×10^{-3}	−2.89	48.1
MCS	1.12×10^{-3}	−3.03	

Therefore, the percentile errors likely refer to the difference between failure probability values. This indicates how significant the discrepancies are when measuring in the analysis process. The smaller percental errors indicate that the predictions are closer to the accepted or original values, while larger percental errors suggest more significant deviations from the actual values. The comparison in Table 5 likely provides insights into the optimal reliability index and represents the accuracy of the system's probability failure predictions.

8. Target Reliability Index Considerations

The reliability-based approach ensures that structures meet a certain level of reliability, exceeding desired target levels through operational design procedures. Establishing standardised procedures for existing steel members, equivalent to new ones, presents challenges but offers the benefits of a reliable framework with built-in margins. Various works have explored appropriate target reliability levels, as seen in ISO 13822 [5], ISO 2394 [6], and JCSS [7], where the consequence of failure determines the target reliability index. Progress in standardisation builds upon a substantial foundation of literature and research, including influential papers by Allen [45] and Ellingwood [25].

Nevertheless, recent investigations such as those by Holicky and Sykora [29], Vrouwenvelder and Vrouwenvelder [46], Tanner et al. [47], Steenbergen et al. [48], and Sýkora et al. [49] have significantly contributed to the standards. Their collective work has been crucial in shaping and improving the standards and guidelines in practice or the field.

ISO 2394 [6] states that the requirements for assessing existing structures are the same as those for designing a new structure. However, a lower target reliability index may be justified for existing structures based on economic, social, and sustainable factors (ISO 13822, Annex F [50]). For lower failure consequences, the target reliability index is 2.3. Moderate failure consequences range from 3.1 to 3.8, while higher failure consequences require a target reliability index 4.3 [8].

FEMA performance assessment guidelines present a more elaborate literature review [51] and offer detailed insights, suggesting a failure probability of less than 5% to avoid severe damage, signifying a hazard that encounters a 99.9% failure probability. Melcher et al. [27] repeated a 5% probability of failure, and a 1.75 reliability index is recommended for existing structural members subjected to earthquake shaking. The most

relevant information is effectively embedded in the LRFD specification. This could serve as background input that the target reliability index ranges from 2.5 to 3.0 [20]. Similarly, JCSS [8] provides structural performance requirements with single and multiple failure probabilities. Additionally, Fischer et al. proposed acceptance criteria of 2.7 to 3.0 for ductile failure members and 2.8 to 3.4 for brittle failure when considering life safety consequences [52].

The comparison presented in this study, as outlined in Table 5, highlights the significance of achieving the proper reliability index level. Additionally, it underlines the alignment with the lower reliability index implied by the acceptance criteria.

The steps for selecting the lower target reliability index range from 2.3 to 2.5 correspond to the consequences of failure, lifetime operation, and the cost of safety measures [7,8,20]. Consequently, these target reliability indices are acceptably lower than the design values of the weakest element in the existing TA–SP connection system, emphasising the relative contributions of plastic and ductile failure mechanisms.

9. Summary and Conclusions

This article introduces a vital breakthrough in research and structural engineering practice. It proposes a new technique for evaluating the reliability of the existing TA–SP connections, viewing significant advances. The proposed methods align with the limit state approaches, engaging in a comparative study of the semi-rigid connection behaviours. In this contribution, the criteria for the existing connection were studied. The practical aspects of a guideline for describing the existing TA–SP connection models were outlined, including integrating the nonlinear FE response into the optimisation process. As a result, both feasible and practical formulations become possible, highlighting the consistency of the parameter power model. Thus, the principal findings of the analysis are outlined as follows:

- The evaluation of the FE method revealed a slight difference in determining the ultimate moment capacity value. The values obtained from the analytical method are approximately 0.78% and 0.84% lower for the initial stiffness and the ultimate moment capacity, respectively, compared to the results obtained from the FE method.
- The overall evaluation exhibited that the differences between the predicted and the FE methods are almost insignificant, demonstrated relatively close results, and effectively captured the ability of the clockwise rotational mechanism of the existing TA–SP connection.

Furthermore, the connection element model was developed to demonstrate the characteristic failure mechanisms of the connected elements. The weakest element is identified during this calibrated phase by associating the applied and plastic resistance moments with the defame gauge length. In these numerical replications of the limit state applications, the actual loading and boundary conditions provided a logical foundation for evaluating existing connection behaviours, and their maximum plastic resistance aids for structural reliability analysis, citing the first-order and second-order reliability methods approximations.

These analysis findings suggest that decreasing the stiffness of element E2 reduces the reliability index by 4% and 6.1% in the SORM and FORM approximations, respectively. Similarly, for another element, E7, the reduction is approximately 5% and 7.8% relative to SORM and FORM. These reductions are considered negligible for the strength limit state. However, from a practical standpoint, ISO 13822, ISO 2394, JCSS, and LRFD specify that seismic design criteria for single components recommend a target reliability index that considers life safety consequences. This recommended range is approximately 2.2% lower than the optimal design reliability index used.

Furthermore, it encompasses the model's primary function, involving the evaluation of optimal results and incorporating the percentile error response for comprehensive analysis. To assess its efficiency, a Monte Carlo Simulation (MCS) with 10,000 samples is used to examine the percentile error sensitivity, revealing a 45.7% difference for SORM and a 70.7%

difference for FORM analysis results. However, the SORM results demonstrate significantly greater efficiency than the FORM results for both element cases. Consequently, it is crucial to appropriately consider the reliability index for the existing TA–SP semi-rigid connection of the weakest elements.

Subsequently, an advanced analysis method is presented for the existing TA–SP connection system's optimisation based on system reliability. Then, the system analysis is distinguished by its two-tiered challenges. The first type involves the design variables of the weakest elements, while the second tier addresses the comprehensive optimisation of the overall connection system, focusing on estimating the system reliability index. The solution unfolds a selection of first- and second-order reliability method procedures, highlighting the critical role of understanding the sensitivity of percentile error tools. This includes the sensitivities related to the system reliability index and addresses the challenge of accurately estimating the system reliability for a stable optimisation process, which leads to the introduction of locked-chain series systems. The correlation between the elements is a crucial parameter, and those with higher strengths significantly contribute to the locked-chain series system. Safety primarily depends on individual elements, particularly the weakest ones in the system. As a result, elements E2 and E7, which are perfectly dependent, exhibited 2.97 and 2.75 reliability indexes, respectively, for the statically determined resistance of CoV of 0.11 and 0.15. These findings led to an optimal reliability index of 2.62, benefiting the system reliability level directory. However, the guidelines suggest a lower target reliability index, ranging from 2.3 to 2.5, considering potential failure consequences, operational lifespan, and the cost of safety measures.

Lastly, the advanced analysis, grounded in the behaviour of the existing TA–SP connection system, yields probabilistic results from a set of 12 samples closely tied to the proposed methodology models. However, these findings may not extend to other structures and connection types. The methodology and concept are foundational for incorporating technical specifications into upcoming design or assessment frameworks. Therefore, the advanced analysis methods of the current study yield more realistic results, as they primarily control the overall system strengths through system reliability analysis. This outcome provides a practical application technique for professionals and researchers involved in verifying the high reliability of aged building systems. Thus, the proposed procedures are custom-made to provide the reliability requirements of existing TA–SP connections and endeavour for meticulous evaluation frameworks in the field.

Limitations: The lack of proper documentation on the original design methods has limited our understanding of the complexity of the existing TA–SP connection. The unique characteristics and behaviours of the TA–SP connections necessitate specific adaptations, which limit the range of possible interventions and increase complexity, which may extend the timeline that requires specialised skills or knowledge.

Recommendations: The findings of the present investigation exclusively address the reliability of the existing TA–SP semi-rigid connection under the clockwise rotational failure mechanism. Despite this, it is highly recommended that the scope of the study be broadened to include the reliability of the TA–SP connection subject to the anticlockwise rotational failure mechanism. This stems from the unique and intricate systemic configurations of the TA–SP connection, which remain unexplored in the present investigation. Furthermore, further research is suggested into the time-dependent reliability of the existing TA–SP connection system that aids in estimating the residual lifespan of the aged buildings that identify potential adaptations.

Author Contributions: Conceptualisations, F.A.Y.; methodology, F.A.Y.; software analysis, F.A.Y.; validation, F.A.Y.; formal analysis, F.A.Y.; investigation, F.A.Y.; data curation, F.A.Y.; writing—original draft preparation, F.A.Y.; visualisation, F.A.Y.; review and editing, F.A.Y.; supervision, C.-Q.L. and S.D.S. All authors have read and agreed to the published version of the manuscript.

Funding: This research received no external funding.

Data Availability Statement: The data presented in this investigation are accessible upon request from the corresponding author.

Acknowledgments: The authors are grateful to the esteemed technical staff of the University of Royal Melbourne Institute of Technology (RMIT) for their cooperation and support in this study.

Conflicts of Interest: The authors declare no conflicts of interest.

Nomenclature

The following symbols are used in this paper:

$\varnothing$	0.6 or 0.8 fillet weld category
Φ^{-1}	Inverse cumulative distribution of the standard function
$\cup$	Union operator in the set
$\cap$	Set intersection operator between two sets
φ_n	Proportional load factor (PLF.)
σ	Standard deviation
μ	Mean value
v	Eigenvalue function scale
β	Reliability index
α_n	Direction cosine at the minimum-distance point
a	Weld throat length and height
A_i	Second-derivative limit state function at the design point
b	Top angle width
b'	Weld section width
B_i	Decomposed diagonalised matrix
CDF	Cumulative distribution function
CoV	Coefficients of variation
d_3	Distance at the centre of rotation
d_4	Distance at the centre of rotation
D_i	Second-derivative performance function
E_i	Event failure in the i-th mode
En	Failure state of the weakest link element
E_M	Elastic modulus
Fi	Shear force function in the i-th element
$f_x(x)$	Probability density function of stochastic variables
$F_{Ri}(r)$	The cumulative distribution function of the strength
f_y	Yield stress
fu	Yield strength
f_{uw}	Yield stress of the weld section
g_1	Gauge length
$g(X)$	Limit state function
h	Height
i	The failure event of the i-th element, (i = 1, 2, . . . n)
ksi	Kilopounds per square inch
k_r	Reduction factor 1.0 for all connection
M_X^*	Moment at the centre of the weald section
M_u	Ultimate moment capacity of the connection
n	Shape parameter of the connection
P_f	Probability of failure
r'^*	Design point at the limit state surface
Ri	Mean value of the plastic moment capacity
$R'i$	Reduced resistance element random variables
Rki	Initial stiffness of the TA–SP connection
S	von Mises criterion stress
s'^*	Design point at the limit state surface

S_i	Mean value of the applied moment for the *i*-th element
S′i	Reduced applied moment random variables
T_d	Seat pad weld throat depth
t_t	Top angle thickness
V_{c1}	Applied compressive force
V_{t1}	Applied tensile force
V^*_{Res}	Applied moment to weld section
V^*_X	Applied moment to x-direction
V^*_Y	Applied moment to y-direction
V_W	Nominal capacity of fillet weld
V^*_Z	Applied moment to z-direction
w	Width
w_n	Fillet weld
x^*	Vector distance point from the origin space
X	Vector of stochastic variables
X_{Fi}	Applied force to the i-th element
X'_i	Reduced random variable for the i-th element
X_i	Tensile force distribution among the elements
X_{Ri}	Resistance element for the i-th element
Y_i	Transformation of a random variable to standard variables
Z_i	Gaussian distribution comprising the chain rules
Zx	Modulus of section
Z_{ew}	Modulus of weld section

References

1. Hardy Cross, M. Analysis of continuous framing by distributing fixed moments. *AISC Am. Soc. Civ. Eng.* **1930**, *96*, 1–10.
2. American Institute of Steel Construction AISC. *Manual of Steel Construction: Load and Resistance Factor Design-LRFD*, 2nd ed.; AISC: Chicago, IL, USA, 1994.
3. *EN 1993*; Eurocode 3: Design of Steel Structures Part 1-1: General Building Rules. European Committee for Standardization: Brussels, Belgium, 2005.
4. Tangaramvong, S.; Tin-Loi, F.; Yang, C.; Gao, W. Interval Analysis of non-linear Frames with Uncertain Connection Properties. *Int. J. Nonlinear Mech.* **2016**, *86*, 83–95. [CrossRef]
5. *ISO 13822*; Bases for Design of Structures Assessment of Existing, ISO TC98/SC2. ISO: Geneva, Switzerland, 2010.
6. *ISO 2394*; General Principles on Structure Reliability, 2nd ed. ISO: Geneva, Switzerland, 1998.
7. JCSS. *Probabilistic Model Code*; Joint Committee on Structural Safety: Zurich, Switzerland, 2001.
8. Richard, R.B.; Abbott, B.J. Versatile elastic-plastic stress and strain formula. *J. Eng. Mech. Div. ASCE* **1975**, *101*, 511515. [CrossRef]
9. Kishi, N.; Chen, W.F. Moment-rotation relations of semi-rigid connections with angles. *J. Struct. Eng. ASCE* **1987**, *116*, 1813–1834. [CrossRef]
10. Colson, A.; Louveau, J.M. Connections Incidence on the Inelastic Behaviour of Steel Structural. In Proceedings of the Euromech Colloquium 174, Palermo, Italy, 10–14 October 1983.
11. Azizinamini, A. Cyclic Characteristics of Bolted Semi-Rigid Steel Beam to Column Connections. Ph.D. Thesis, University of South Carolina, Columbia, SC, USA, 1985.
12. Bjorhovde, R.; Colson, A.; Brozzetti, J. Classification system for beam-to-column connections. *J. Struct. Eng. AISC* **1990**, *116*, 3059–3076. [CrossRef]
13. Pekcan, G.; Mander, J.B.; Chen, S.S. Experimental & analytical study of low-cycle fatigue behaviour of semi-rigid top and seat angle connections. *AISC Eng. J.* **1995**, *31*, 111–122.
14. Faella, C.; Piluso, V.; Rizzano, G. *Structural Steel Semi-Rigid Connections Theory Design, and Software*; Engineering, Materials Science; CRC Press: Boca Raton, FL, USA, 1999.
15. Ahmed, A.; Kishi, N.; Matsuoka, K.; Komuro, M. Nonlinear analysis on prying of top- and seat-angle connections. *J. Appl. Mech.* **2001**, *4*, 227–236. [CrossRef]
16. Pirmoz, A.; Seyed, K.; Mohammadrezapour, A.; Saedi, D.E. Moment-rotation behaviour of bolted top-seat angle connections. *J. Constr. Steel Res.* **2009**, *65*, 973–984. [CrossRef]
17. Smitha, M.S.; Babu, S. Behaviour of top and seat angle semi-rigid connections. *J. Inst. Eng. India A* **2014**, *94*, 153–159. [CrossRef]
18. ABAQUS. *CAE User's Manuals, Version 6.14*; Hibbitt Karlsson & Sorensen: Pawtucket, RI, USA, 2014.
19. Yonis, F.A.; De Saliva, S. *Investigating the TA-SP Semi-Rigid Connection through Finite Element Method Validation via Moment-Rotation Analysis, Practice Periodical on Structural Design and Construction*; ASCE: Reston, VA, USA, 2024; Under review.
20. von Mises, R.E. Mechanik der Festen Körper im Plastisch-Deformablen Zustand. Corpus ID: 138864271. Available online: https://resolver.sub.uni-goettingen.de/purl?252457811_1913%7Clog53 (accessed on 27 May 2024).

21. *ANSI/AISC 360*; Specification for Structural Steel Buildings. American Institute of Steel Construction: Chicago, IL, USA, 2010.
22. Drucker, D.C. The effect of shear on the plastic bending of beams. *J. Appl. Mech. ASME* **1956**, *23*, 509–514. [CrossRef]
23. Tresca, H. Sur L'ecoulement des Corps Solides Soumis a de Fortes Pressions. *Comptes Rendus L'académie Sci.* **1864**, *59*, 754.
24. *AS 4100*; Australian Standard, Steel Structures. Standards Australia: Sydney, Australia, 2020.
25. Ellingwood, B. Reliability-based condition assessment and LRFD for existing structures. *Struct. Saf.* **1996**, *18*, 67–80. [CrossRef]
26. Fisher, J.; Ravindra, M.; Galambos, T. Load and resistance factor design criteria for connection. *J. Struct. Div. ASCE* **1978**, *104*, 1427–1441. [CrossRef]
27. Galambos, T.; Ravindra, M. Properties of steel for use chapter in LRFD. *J. Struct. Div. ASCE* **1968**, *104*, 1459–1468. [CrossRef]
28. Kennedy, D.J.L.; Gad Aly, M. Limit states design of steel structures performance factors. *Can. J. Civ. Eng.* **1980**, *7*, 45–77. [CrossRef]
29. Melchers, R.E.E. *Structural Reliability Analyses and Prediction*, 1st ed.; Jonh Wiley & Sons, Inc.: Chichester, NY, USA, 2017.
30. Sýkora, M.; Holický, M.; Marková, J. Target reliability levels for assessment of existing structures. In *Applications of Statistics and Probability in Civil Engineering*; Faber, M.H., Köhler, J., Nishijima, K., Eds.; CRC Press/Balkema: Boca Raton, FL, USA, 2011; pp. 1048–1056.
31. Freudenthal, A. Safety, reliability and structural design. *J. Struct. Div. ASCE* **1961**, *87*, 1–16. [CrossRef]
32. Weibull, W. A statistical theory of the strength of the material. *Proc. R. Sweden. Inst. Eng. Res.* **1939**, *15*, 1887–1979.
33. Cornell, C. A probability-based structural code. *Am. Concr. Inst. Struct. J.* **1969**, *66*, 974–985.
34. Breitung, K. Asymptotic Approximations for Multinormal Integrals. *J. Eng. Mech. ASCE* **1984**, *110*, 357–366. [CrossRef]
35. Bucher, C.G. Adaptive Sampling an iterative, fast Monte Carlo procedure. *J. Struct. Saf.* **1988**, *5*, 119–126. [CrossRef]
36. MATHCAD 15. *MATHCAD User's Manuals*; P.T.C.: Boston, MA, USA, 2014.
37. Halder, A.; Mahadevan, S. *Probability, Reliability and Statistical Methods in Engineering Design*; Jonh Wiley & Sons, Inc.: New York, NY, USA, 2000.
38. Ang, A.; Tang, W. *Probability Concepts in Engineering Planning and Design: Vol. I, Basic Principles*; John Wiley & Sons: New York, NY, USA, 1978; p. 409.
39. Hasofer, A.M.; Lind, N.C. An exact and invariant first-order reliability format. *J. Eng. Mech.* **1974**, *100*, 111–121.
40. Rackwitz, R.; Flessler, B. Structural reliability under combined random load sequences. *J. Comput. Struct.* **1978**, *9*, 489–494. [CrossRef]
41. Rosenblatt, M. Remarks on a multivariate transformation. *Ann. Math. Stat.* **1952**, *23*, 470–472. [CrossRef]
42. Bastidas-Arteaga, E.; Soubra, A.-H. Reliability Analysis Methods. In *ALERT Doctoral School, Stochastic Analysis and Inverse Modelling*; Hicks, M.A., Jommi, C., Eds.; Grenoble, University of Nantes—GeM Laboratory—UMR CNRS 6183: Nantes, France, 2014; pp. 53–77. ISBN 978-2-9542517-5-2. HAL Id: in2p3-01084369; Available online: https://www.researchgate.net/publication/281372166 (accessed on 27 May 2024).
43. Zhang, J.; Du, X. A second-order reliability method with first-order efficiency. *Am. Soc. Mech. Eng. ASME* **2010**, *132*, 101006. [CrossRef]
44. Thoft-Christensen, P.; Dalsgård Sørensen, J. Reliability of structural systems with correlated elements. *J. Appl. Math. Model.* **1982**, *6*, 171–178. [CrossRef]
45. Allen, D.E. Limit states criteria for structural evaluation of existing buildings. *Can. J. Civ. Eng.* **1991**, *18*, 995–1004. [CrossRef]
46. Vrouwenvelder, T.; Scholten, N. Assessment criteria for existing structures. *J. Struct. Eng. Int. IABSE* **2010**, *20*, 62–65. [CrossRef]
47. Tanner, P.; Sarache, C.L. Semi-probabilistic models for the assessment of existing concrete structures. In Proceedings of the 11th International Conference on Applications of Statistics and Probability in Civil Engineering, Zurich, Switzerland, 1–4 August 2011.
48. Steenbergen, R.; Sýkora, M.; Diamantidis, D.; Holický, M. Economic and human safety reliability levels for existing structures. *Struct. Concr.* **2015**, *16*, 323–332. [CrossRef]
49. Sýkora, M.; Diamantidis, D.; Holický, M.; Jung, K. *Life-Cycle of Structural Systems, Target Reliability for Existing Structures Considering Economic and Societal Aspects*, 1st ed.; Routledge Taylor & Francis: London, UK, 2016. [CrossRef]
50. *ISO13822: 2010/SANS 13822:2016*; Bases for Design of Structures. Assessment of Existing Structures. International Organisation for Standardisation/South African National Standard: Geneva, Switzerland, 2016.
51. Federal Emergency Management Agency (FEMA). *Interim Guidelines Evaluation, Repair, Modification and Design of Welded Steel Moment Frame*; Report (SAC Joint Venture), No. SAC-95-02; FEMA: Washington, DC, USA, 1995.
52. Fischer, K.; Viljoen, C.; Köhler, J.; Faber, M.H. Optimal and acceptable reliabilities for structural design. *J. Struct. Saf.* **2019**, *76*, 149–161. [CrossRef]

Disclaimer/Publisher's Note: The statements, opinions and data contained in all publications are solely those of the individual author(s) and contributor(s) and not of MDPI and/or the editor(s). MDPI and/or the editor(s) disclaim responsibility for any injury to people or property resulting from any ideas, methods, instructions or products referred to in the content.